American Journal of Energy Research, 2023, Vol. 11, No. 2, 93-99
Available online at http://pubs.sciepub.com/ajer/11/2/4
Published by Science and Education Publishing
DOI:10.12691/ajer-11-2-4

Effects of Transport Window Layers on All-inorganic $CsPbI_{3-x}Br_x$ Perovskites Based Solar Cells

Alioune Sow*, Saliou Seck, Mamadou Salif Mane, Amadou Ndiaye, Bachirou Ndiaye, El-Hadji Mamadou Keita, Babacar Mbow, Cheikh Sene

Physics Department, Faculty of Sciences and Technology, Laboratory of Semiconductors and Solar Energy, University Cheikh Anta Diop, Dakar Country
*Corresponding author: sowalioune902@gmail.com

Received March 22, 2023; Revised April 25, 2023; Accepted May 14, 2023

Abstract All-inorganic perovskites based on $CsPbI_{3-x}Br_x$ are promising halides for use in efficient photovoltaic devices due to their high stability. This generated a tremendous research interest from the scientific community to move towards this class of materials. However, perovskite solar cells based on $CsPbI_{3-x}Br_x$ have not yet achieved the expected conversion efficiencies compared to their hybrid counterpart. In this work we used SCAPS 1D to model the all-inorganic $CsPbI_{3-x}Br_x$ based solar cell, investigate and discuss the limitations of the device in order to improve its conversion efficiency. For this purpose, we used the normal (n-i-p) configuration with *Al/ETL/*$CsPbI_{3-x}Br_x$*/HTL*/ITO structuring. By varying the inorganic transport layers HTL and ETL, our study revealed that the best HTL/ETL combination is Cu_2O as HTL and SnO_2 as ETL. We otherwise have shown that acceptor and donor doping of Cu_2O and SnO_2 respectively offers a mean to reduce recombination in the device. The study showed that the acceptor (N_A=10^{18}cm^{-3}) and donor (N_D=10^{17}cm^{-3}) doping rates are the best dopant values for the cell. By optimizing the various study parameters, we obtained a high-performance normal structure PSC with a conversion efficiency (PCE) of 17.87%.

Keywords: *Perovskite, absorber, hole transport layer, electron transport layer, solar cell*

Cite This Article: Alioune Sow, Saliou Seck, Mamadou Salif Mane, Amadou Ndiaye, Bachirou Ndiaye, El-Hadji Mamadou Keita, Babacar Mbow, and Cheikh Sene, "Effects of Transport Window Layers on All-inorganic $CsPbI_{3-x}Br_x$ Perovskites Based Solar Cells." *American Journal of Energy Research*, vol. 11, no. 2 (2023): 93-99. doi: 10.12691/ajer-11-2-4.

1. Introduction

In a decade, perovskite-based solar cells have grown dramatically with a rapid improvement in efficiency from 3.8% [1,2,4-8,10,12] in 2009 to 25.5% [9,10,14,19] in 2021, making perovskites a new family of materials with great promise for photovoltaic. This exceptional progress has sparked a great deal of interest from the scientific community to focus more on perovskites. However, several challenges need to be addressed in order to consider a future commercialization of perovskite-based photovoltaic (PV) devices. These include lead toxicity, a rather limited understanding of physical processes such as hysteresis of I-V characteristics, and especially the stability problems of hybrid perovskite-based devices. It is therefore essential to succeed in stabilizing these devices in order to achieve perovskite materials based solar cells, which perform well, have a very long service life and comply with environmental standards. The stability problems noted in the hybrid perovskites have thus redirected researchers towards all-inorganic materials. Compared to hybrid perovskites, all-inorganic perovskites have demonstrated better thermal stability [11] and much more suitable carrier transport properties to theoretically give higher efficiencies. However, experimental efficiencies provided by all-inorganic perovskite-based solar cells are still far below those obtained by their hybrid counterpart. The poor performance of all-inorganic perovskites compared to the theoretical limit [13] may be due to intrinsic problems such as high defect densities, energy level mismatch, choice of transport layers used in the device processing, acceptor and donor doping levels, etc... These shortcomings could be overcome by a modelling investigation of the perovskite based photovoltaic device together with an appropriate choice of the perovskite material and electrons and holes transport layers.

In this simulation study we used $CsPbI_{3-x}Br_x$ as the perovskite material with several materials as electron and hole transport layers (HTL and ETL). Our main objective being to obtain highly stable all-inorganic PSCs (PSCs) composed not only of the inorganic halide perovskite absorber, but also of inorganic hole and electron transport window layers. For this purpose we first performed the validation of our solar cell model on the normal configuration *Al/ETL/*$CsPbI_{3-x}Br_x$*/HTL*/ITO by comparing

our experimental results with those obtained by other research groups. Then, several inorganic materials are tested as electron and hole transport layers. These materials included TiO_2 and SnO_2 as electron transport layer (ETL) with ZnO taken as reference material, and CuI and Cu_2O as hole transport layer with NiO_x as reference material. Finally, investigation on the acceptor and donor doping rate of the HTL and ETL layers was carried out for the best transport layers in order to maximize the conversion efficiency of the device.

2. The Solar Cell Device Structure

SCAPS-1D program developed by GANT University [12,14] for the numerical modelling of thin film solar cells have been used. For this purpose, it is imperative to solve the Poisson equation (1) and the continuity equations of electrons (2) and holes (3), respectively:

$$\frac{d}{dx}\left(\varepsilon(x)\frac{d\Psi}{dx}\right)=q\left[\begin{matrix}p(x)-n(x)+N_D^+(x)\\-N_A^-(x)+p_t(x)-n_t(x)\end{matrix}\right] \quad (1)$$

$$\nabla j_n = q\left[R_n - G_n + \frac{\partial n}{\partial t}\right] \quad (2)$$

$$\nabla j_p = q\left[R_p - G_p + \frac{\partial p}{\partial t}\right] \quad (3)$$

In these equations n and p are the free electrons and holes concentrations, respectively, n_t and p_t being the trapped electrons and holes concentrations and N_D^+ and N_A^- representing the ionized donor and acceptor doping concentrations, respectively.

By solving these three equations, the modelling parameters are obtained. The normal (n-i-p) planar PSCs used in the simulation consists in Al/ $ZnO/CsPbI_{3-x}Br_x/NiO_x$/ITO as shown in Figure 1, where the $CsPbI_{3-x}Br_x$ absorber is sandwiched between a $p-NiO_x$ layer as the HTL and a $n-ZnO$ layer the ETL. An Indium Tin Oxide (ITO) layer is applied as a back contact and an aluminum metal (Al) layer as a front contact. The material parameters used are taken from the literature and are summarized in Table 1.

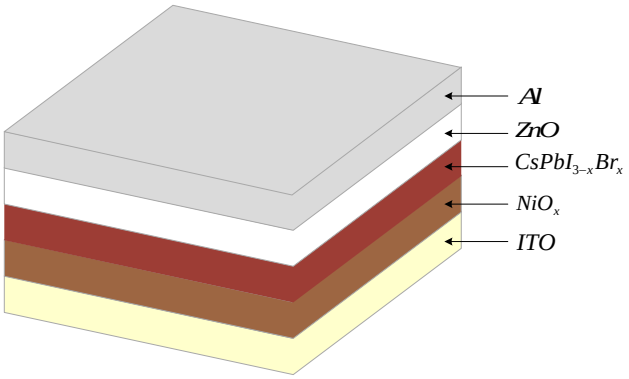

Figure 1. Device structure of the $CsPbI_{3-x}Br_x$ perovskite based solar cell

In the table, N_C and N_V are the effective conduction-band and valence-band densities, N_A and N_D are the acceptor and donor densities, μ_p and μ_n are the hole and electron mobilities, N_t is the defect density, χ is the electron affinity and ε_r is the relative permittivity of the perovskite material.

Table 1. Inorganic materials and input parameters used for modelling the perovskite-based solar cell

	NiO_x	$CsPbI_{3-x}Br_x$	ZnO
$N_A(cm^{-3})$	10^{18} [16]	-	-
$N_D(cm^{-3})$	-	10^{13}	10^{18} [21]
ε_r	10^{18} [21]	7.43 [10]	9.0 [12,16]
χ(eV)	1.8 [16]	3.76 [10]	4.0 [12]
E_g(eV)	3.25 [3]	1.72 [17]	3.3 [18]
$\mu_n(\frac{cm^2}{V}/s)$	0.001 [16]	6.83	100 [21]
$\mu_p(\frac{cm^2}{V}/s)$	0.001 [16]	6.83	25 [12]
$N_t(cm^{-3})$	1.0010^{15} [22]	4.6110^{15}	1.0010^{16}
$N_C(cm^{-3})$	2.210^{18} [15]	2.210^{18}	2.210^{18}
$N_V(cm^{-3})$	1.810^{19}	1.810^{19} [16]	1.810^{19}
Thickness(nm)	80 [16]	490 [20]	70 [16]

In this study, we set for the $CsPbI_{3-x}Br_x$ absorber, the energy band gap at 1.72 eV [17], the thickness at 490 nm [20] and the initial defect density at $4.6110^{15}\,cm^{-3}$. Work functions of back and front contact are 4.8 eV (ITO) and 3.3 eV (Al), respectively. The simulation study was done in the standard AM 1.5G ($100W/m^2$, T= 300K).

3. Results and Discussions

3.1. Validation of the Device Model

In our reference solar cell model, ZnO and NiO_x are used as ETL and HTL, respectively together with $CsPbI_{3-x}Br_x$ perovskite as the absorbing material. The input parameters for the simulation are those shown in Table 1. The current density-voltage (J-V) curve obtained is shown in the Figure 2.

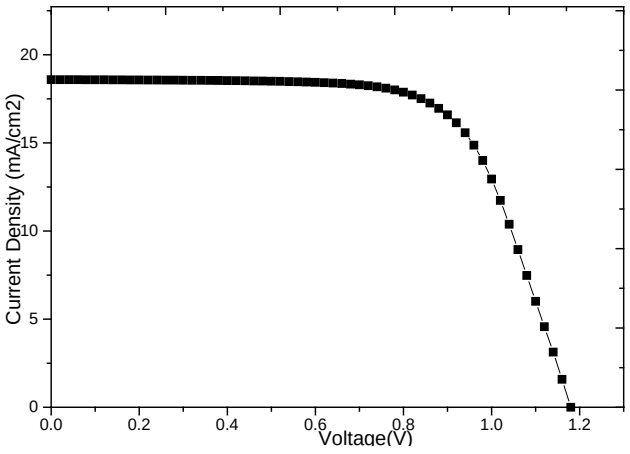

Figure 2. J-V characteristics obtained by simulation using input parameters in Table 1

The extracted results from the above curve of our solar cell modeling are compared in Table 2 with experimental data from the literature [20]. Our device model shows a conversion efficiency (PCE) of 14.87% corresponding to a

short-circuit density of 18.72 mA/cm^2, an open-circuit voltage (V_{oc}) of 1.18 V and a fill factor (FF) of 67.44%, which are close to the experimental values reported in 2021 by Jin Hyuck Heo (see Table A1) [20]. This preliminary step in this work allowed us to validate both our device model and the values of the parameters used in the simulation. It therefore makes it possible to use the model to investigate and analyze the various other parameters of the solar cell.

Table 2. Comparison of simulation and experimental results of the perovskite based solar cell

	V_{oc} (V)	$J_{sc}(mA/cm^2)$	FF(%)	PCE(%)
Experimental	1.20	15.62	79.06	14.82
Simulation	1.18	18.72	67.44	14.87

3.2. Influence of the Hole Transport Layer (HTL) on the Device Performance

The hole transporting layer (HTL) plays an important role in perovskite based solar cells (PSCs). Compared to organic HTL, inorganic HTLs have advantages of simple preparation, good chemical stability, high hole mobility and low cost, making them potential candidates for use in stable PSCs. In this section, various HTL are used with a ZnO film as ETL. The input parameters used in the simulation are given in Table 3.

Table 3. Input physical parameters of the HTL materials

	NiO_x[10,12]	CuI[12,14]	Cu_2O[12,14]
$N_A(cm^{-3})$	10^{18}	10^{18}	10^{18}
$N_D(cm^{-3})$	-	-	-
ε_r	11.75	6.5	7.1
χ(eV)	1.8	2.1	3.2
E_g(eV)	3.25	3.10	2.17
$\mu_n(\frac{cm^2}{V}/s)$	0.001	100	200
$\mu_p(\frac{cm^2}{V}/s)$	0.001	43.9	80
$N_t(cm^{-3})$	10^{15}	10^{15}	10^{15}
$N_C(cm^{-3})$	$2.2 10^{18}$	$2.2 10^{18}$	$2.2 10^{18}$
$N_V(cm^{-3})$	$1.8 10^{19}$	$1.8 10^{19}$	$1.8 10^{19}$
Thickness(nm)	80	80	80

Figure 3 shows the external quantum efficiency (EQE) plots obtained with the various HTLs. A broad spectral response is observed up to a 750 nm whatever the HTLs used. We also notice from Figure 3 that the external quantum efficiency is not really influenced by the HTL nature. This is due to the fact that the hole transport layer is located at the back of the absorbing layer which causes little influence on the optical absorption. The energy level diagram (Figure 4) shows a good alignment of the HTL energy levels with that of the $CsPbI_{3-x}Br_x$ absorbing layer. However better aligment is pointed out with the Cu_2O HTL which shows that the Cu_2O performs better as HTL than the other materials (NiO_x and CuI). Figure 5 shows the current density vs. voltage (J-V) characteristics of the perovskite based solar cell as a function of the HTL nature. The solar cell performances are listed in Table 4. These results and those from figure 5confirm that Cu_2O is the best HTL material used in the device with a conversion power of 17.70%, a fill factor (FF) of 79.98%, an open circuit-voltage (V_{oc}) of 1.18V and a short-circuit current density J_{sc} of 18.77mA/cm^2. The high efficiency obtained with Cu_2O is partly due to the fact that it has the best alignment of its valence band with the absorbing layer and therefore has the most occupied molecular orbital (HOMO) than the other HTLs.

Table 4. Solar cell performance for different HTLs

	V_{oc} (V)	$J_{sc}(mA/cm^2)$	FF(%)	PCE(%)
NiO_x	1.18	18.72	67.44	14.87
CuI	1.16	18.73	79.14	17.19
Cu_2O	1.18	18.77	79.98	17.70

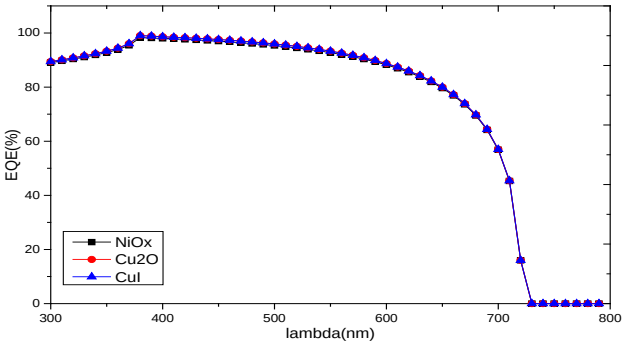

Figure 3. EQE plots for the $CsPbI_{3-x}Br_x$ based solar cell with the various HTLs.

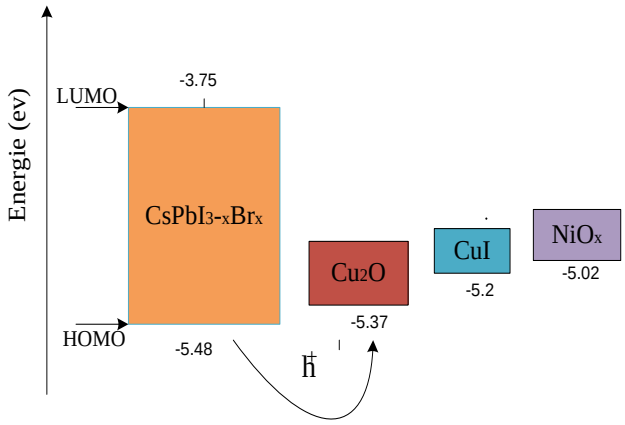

Figure 4. Band alignment between the $CsPbI_{3-x}Br_x$ absorber and the different HTLs

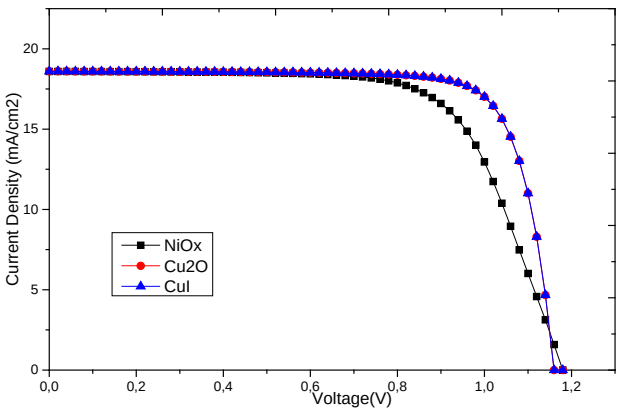

Figure 5. J-V plots for the $CsPbI_{3-x}Br_x$ based solar cell with the various HTLs

3.3. Effect of the Electron Transport Layers on the Device Performance

We have set Cu_2O as the HTL and we will study the effect of several ETL films (TiO_2, ZnO and SnO_2) in this section. The parameters used for the ETLs are listed in Table 5.

Table 5. The parameters of the different ETLs

	TiO_2 [10,12]	ZnO [12,21]	SnO_2[12,23]
$N_A(cm^{-3})$	-	-	-
$N_D(cm^{-3})$	10^{18}	10^{18}	10^{18}
ε_r	9	9	9
χ(eV)	4	4	4
E_g(eV)	3.2	3.3	3.5
$\mu_n(\frac{cm^2}{V}/s)$	20	100	20
$\mu_p(\frac{cm^2}{V}/s)$	10	25	10
$N_t(cm^{-3})$	10^{15}	10^{16}	10^{15}
$N_C(cm^{-3})$	10^{21}	2.210^{18}	4.3610^{18}
$N_V(cm^{-3})$	2.10^{20}	1.810^{19}	2.610^{21}
Thickness(nm)	70	70	70

Figure 6 highlights the external quantum efficiency (EQE) of solar cells with different ETL. The external quantum efficiency plot is essentially composed of two parts. Between 300 nm and 400 nm, a very slight increase in external quantum efficiency is observed up to a maximum value of 400 nm. In this wavelength range, the solar cell with TiO_2 as ETL has a slightly better response than its homologues. But from 400 nm, the responses of the three ETLs remain almost identical throughout this wavelength range.

Table 6. Solar cell performances for different ETLs

	V_{oc} (V)	$J_{sc}(mA/cm^2)$	FF(%)	PCE(%)
TiO_2	1.21	18.76	75.68	17.17
ZnO	1.18	18.77	79.98	17.70
SnO_2	1.19	18.77	81.98	17.75

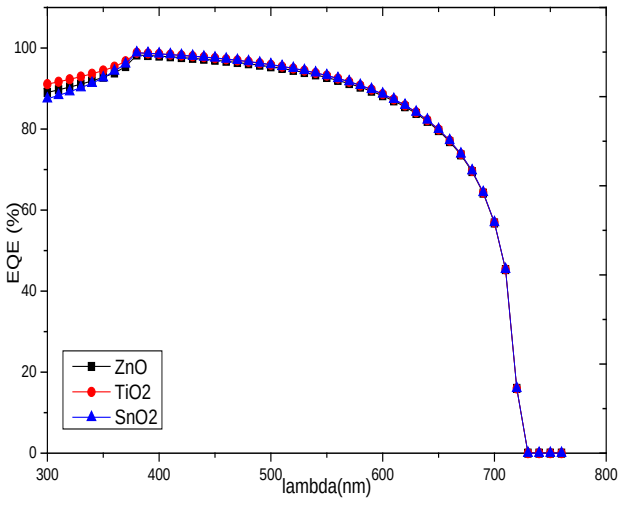

Figure 6. EQE plots for the $CsPbI_{3-x}Br_x$ based cell with the different ETLs

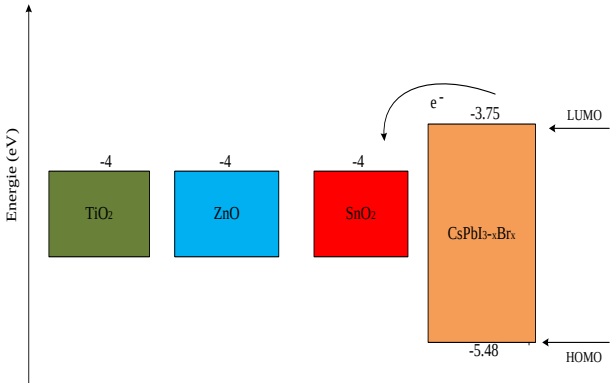

Figure 7. Band alignment between the $CsPbI_{3-x}Br_x$ absorber and the different ETLs

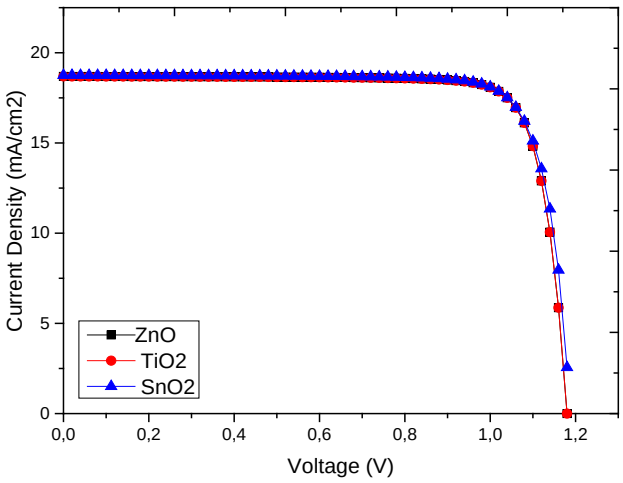

Figure 8. J-V characteristics of the $CsPbI_{3-x}Br_x$ based solar cell using different ETLs

Figure 8 shows the J-V characteristics of the solar cells using TiO_2 , ZnO and SnO_2 as ETL and Table 5 summarizes the performances of these solar cells. The photovoltaic conversion efficiencies (PCE) are 17.17%, 17.70% and 17.75%, respectively. These results which are very little different are due to a perfect alignment of the material conduction band with that of the molecular orbit (LUMO) of the absorber $CsPbI_{3-x}Br_x$ layer (Figure 7), which facilitates electrons transport between the absorber and the ETL. However, simulation results (Table 6) show that the solar cell with SnO_2 as ETL has a better conversion efficiency.

We can see that there is not much difference in the J-V curves (Figure 5a) for the ETLs used and they have almost the same spectral response width which is around 720 nm (see Figure 5b).

3.4. Effect of the Acceptor Doping Concentration (N_A) on the Perovskite Layer (HTL/PSK)

To study the effect of doping the HTL layer, the acceptor concentration was varied from 10^{13} to $10^{18}cm^{-3}$ and the results are shown in Figure 9, Figure 10 and Figure 11. It can be seen in Figure 10b that the maximum yield of 17.70 % is achieved for the acceptor concentration of $10^{18}cm^{-3}$. It is important to note that the

efficiency (Figure 10a), the fill factor (Figure 10b) and the short-circuit current density (Figure 10d) of the cell increase with the increase of the acceptor doping concentration. On the other hand, figure (Figure 10c) shows that from 10^{13} to $10^{17} cm^{-3}$, the open circuit voltage of the $CsPbI_{3-x}Br_x$ solar cell decreases with the increase of the acceptor concentration doping rate. This can be explained by the fact, the acceptor doping in the HTL layer avoids the recombination phenomenon in the HTL layer (Cu_2O). Moreover, the electrons that were in the valence band at the HTL will migrate and find holes resulting in the increase of the electrical parameters (J_{sc}, FF and PCE). From 10^{17} to $10^{18} cm^{-3}$, the open circuit voltage increases very little and this will have no effect on the PCE efficiency (Figure 10a) and the fill factor (Figure 10b) of the solar cell. As can be seen in Figure 9, the J-V curves are almost identical under low acceptor density. However, when N_A is greater or equal to $10^{17} cm^{-3}$, the current density decreases while V_{oc} slightly increases. For low N_A values ($10^{13} - 10^{14} cm^{-3}$) a high electric field is formed across the absorber, which is beneficial for the separation and collection of light-generated carriers leading to a higher current density [12]. In Figure 11 which shows the external quantum efficiency (EQE) of the $Cu_2O/CsPbI_{3-x}Br_x$ cell as a function of acceptor doping concentration, it can be seen that doping the HTL layer with acceptor has no effect on the responses of the solar cells. This is simply because the HTL layer (Cu_2O) is at the back contact of the absorber layer.

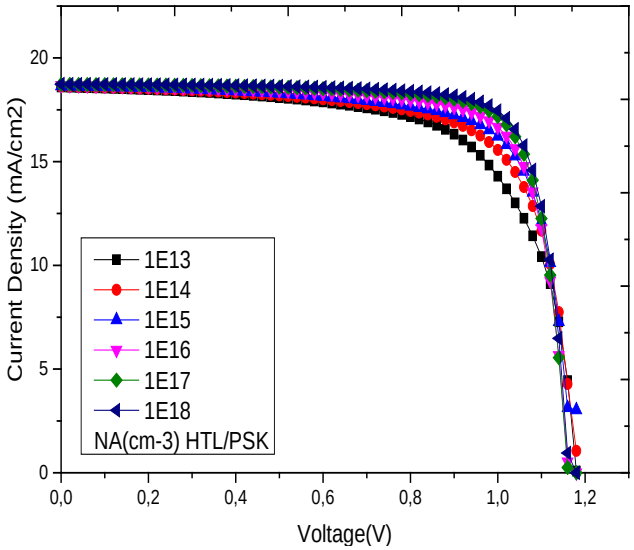

Figure 9. J-V characteristics as a function of acceptor doping concentration

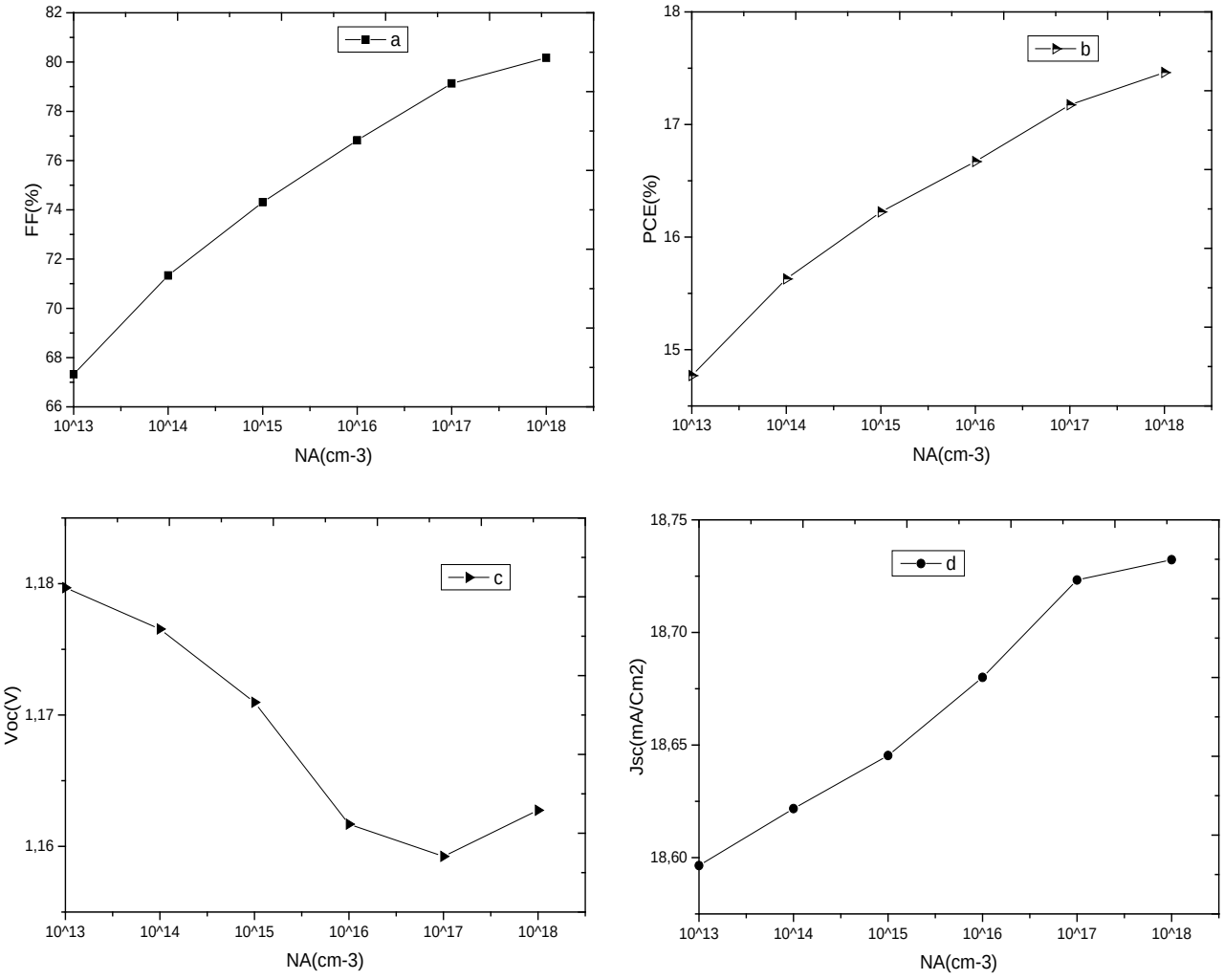

Figure 10. Effect of acceptor concentration on (a) FF, (b) PCE, (c) V_{OC} and (d) J_{SC}

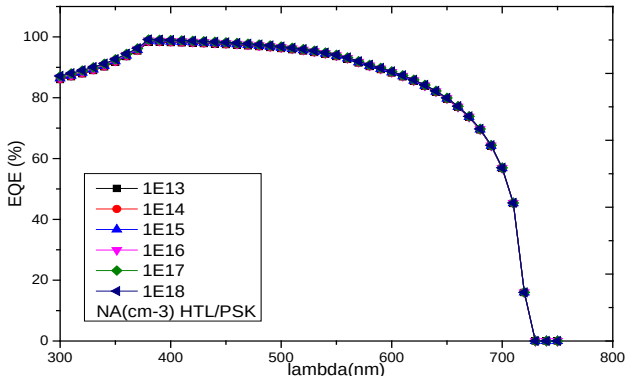

Figure 11. EQE of the perovskite based-solar cell as a function of acceptor doping

3.5. Effect of the Donor Concentration (N_D) on the ETL/PSK Perovskite Layer

In this section, SnO_2 which has shown better performance as ETL is used in the simulation. As already highlighted in Figure 6, the upper energy level of SnO_2 being very close to that of the $CsPbI_{3-x}Br_x$ absorber, allows good electron transport to the back contact and prevents holes from escaping. The results of the effect of N_D donor doping of ETL/PSK are shown in Figure 12, Figure 13 and Figure 14. As can be observed in Figure 12a, the open circuit voltage remains almost unchanged for N_D values below 10^{15}cm^{-3}. Between 10^{13}cm^{-3} and 10^{15}cm^{-3}, donor doping level has no effect on the open circuit voltage. The recombination rate neither increases nor decreases in this doping level range. Above 10^{15}cm^{-3}, increase in the donor doping level causes a rapid drop in the open circuit voltage resulting in a reduction of carriers recombination between the ETL/PSK layers. An increase in the fill factor is noted from 10^{15}cm^{-3} onwards (Figure 12 c), which then tends toward saturation for even higher donor doping rates.

This can be attributed to an increase in the ETL conductivity and also to a decrease in the series resistance of the solar cell. The PCE of the solar cell follows the same tendency as the fill factor (Figure 12 b) and reaches its maximum value at an N_D value of 10^{17}cm^{-3} which corresponds to a conversion efficiency of 17.87%. The short circuit current density curve follows the same behaviour as the PCE and FF curves up to 10^{17}cm^{-3} (Figure 12 d). From this point onwards, the donor doping rate of the ETL layer causes a drastic decrease in Jsc and the solar cell efficiency. The simulated J-V curves as a function of ETL doping concentration are shown in Figure 13. This plots indicates that the J-V characteristics as well the corresponding photovoltaic parameters (J_{sc}, V_{oc}, FF et PCE) are almost similar for doping levels below $10^{15} cm^{-3}$. From $10^{15} cm^{-3}$ onwards, the increase in the donor doping rate of the ETL layer les a progressive improvement of the J-V characteristic shape. On the other hand, it can be noted that a better spectral response is observed between 300 nm and 400 nm when the donor doping rate takes a value of $10^{17} cm^{-3}$. Above 400 nm, the donor doping of the ETL layer has no effect on the external quantum efficiency of the cell (Figure 12). It is also noted for open circuit voltage values between 0.8 and 1.1 V (see Figure 10), the donor doping of the ETL layer leads to an increase in the series resistance of the cell. The highest resistivity of the cell is reached when the doping is $10^{18} cm^{-3}$, thus it can be deduced that this value is not adequate to reduce the recombinations in the $SnO_2 / CsPbI_{3-x}Br_x$ junction. Therefore, the simulation results of the ETL layer (SnO_2) show that the donor doping rate equal to $10^{17} cm^{-3}$ is more favorable for the SnO_2 layer presented better performance for a photovoltaic device.

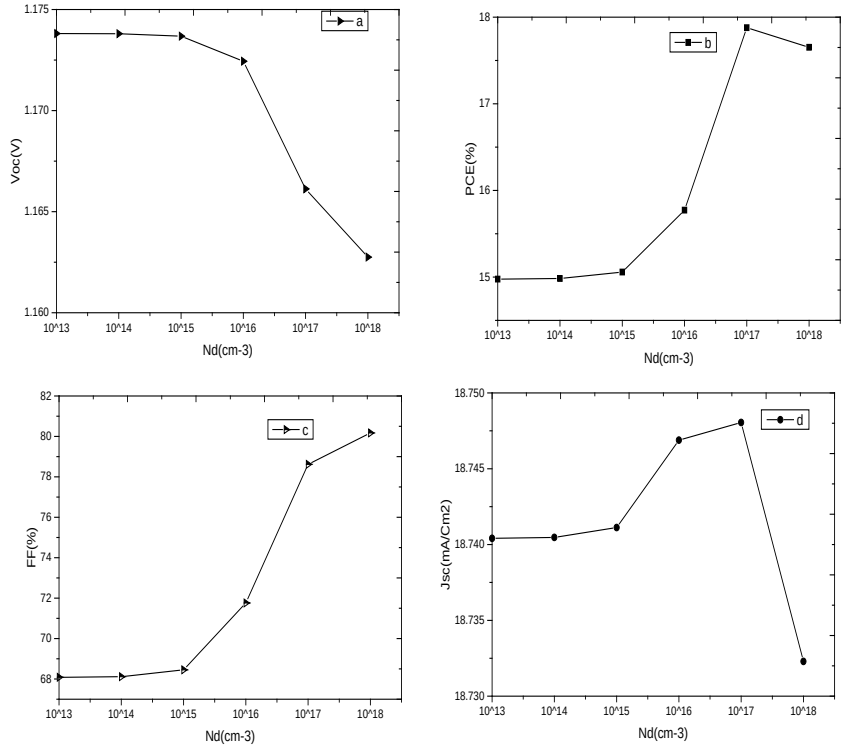

Figure 12. Effect of donor concentration (a) FF, (b) PCE, (c) V_{oc} and (d) J_{sc}

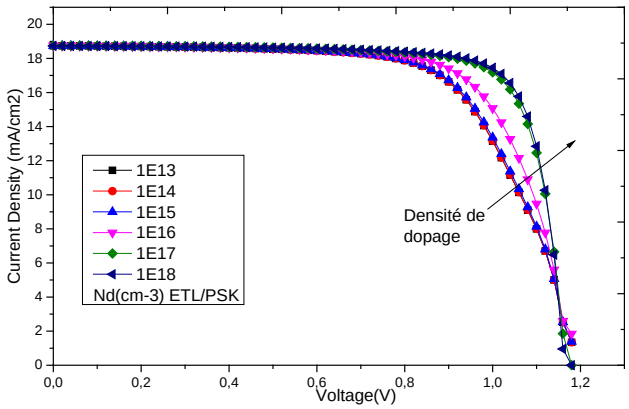

Figure 13. J-V characteristics as a function of donor doping concentration

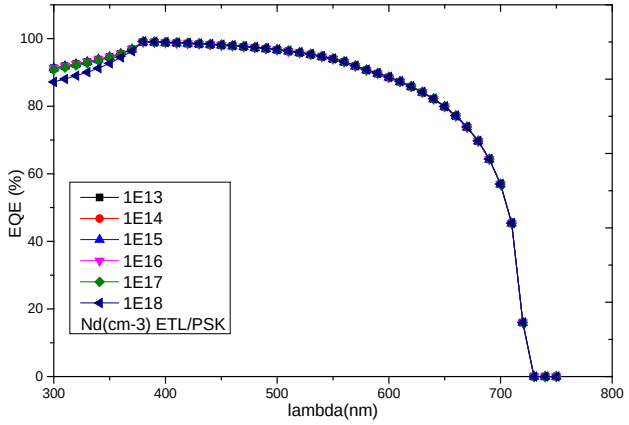

Figure 14. Spectral response of the cell as a function of donor doping

4. Conclusion

In this work, the inorganic $CsPbI_{3-x}Br_x$ absorber is studied and numerically optimized by SCAPS-1D software using the (n-i-p) setup device with Al/ETL/$CsPbI_{3-x}Br_x$/HTL/ITO structuring. First, we fixed the ETL (ZnO) layer and varied the HTL layer. For the different inorganic hole transport layers used (NiO_x, Cu_2O and CuI), the study revealed that Cu_2O is the best candidate due to its good alignment of its valence band with that of the absorber. Subsequently, by setting the best HTL (Cu_2O) and varying the ETLs (ZnO, TiO_2 and SnO_2), the modelling results showed that with the SnO_2 layer, the device gives better photovoltaic conversion efficiency. So the best HTL/ETL combination is given by Cu_2O and SnO_2 layers respectively. With their better acceptor and donor doping rates of the carrier transport layers, we optimized the conversion efficiency of the $CsPbI_{3-x}Br_x$ absorber, which increases to 17.87%. Considering the results obtained with the simulation, we can refer to it for the experimental development of promising devices based only on all-inorganic perovskites.

References

[1] Yuqing Zhang, Cuncun Wu, Duo Wang, Zehao Zhang, Xin Qi, Ning Zhu, Ganghong Liu, Xiangdong Li, Haozhe Hu, Zhijian Chen, Lixin Xiao, and Bo Qu, "High efficiency (16.7 %) of cesium bromium- passivated all-inorganique *CsPbI$_2$Br* perovskite solar cell", Solar RRL, 3, 1900254, 1-8 (2019).

[2] Kaijie Wang, Ye Tian, Heng Jiang, Meng Chen, and Shuangyan Xu, "Surface Treatment on Nickel Oxide to Enhance the Efficiency of Inverted Perovskite Solar Cells", International Journal of Photoenergy, 4360816, 7 (2019).

[3] Jiang Yang, Qiong Zhang, Jinjin Xu, Hairui Liu, Ruiping Qin, Haifa Zhai, Songhua Chen and Mingjian Yuan, "All-inorganic perovskite solar cells based on *CsPbIBr$_2$* and metal oxide transport layers with improved stability", Nanomaterials, 9, 16 (2019).

[4] Saad Ullah, Ping Liu, Jiaming Wang, Peixin Yang, Linlin Liu, Shi-E. Yang, Haizhong Guo, Tianyu Xia, Yongsheng Chen, "Optimizing the working mechanism of the *CsPbBr$_3$* based inorganic perovskite solar cells for enhanced efficiency", Solar Energy, 209, 79-84 (2020).

[5] Nabonswende Aida Nadege Ouedrago, Yichuan Chena, Yue Yue Xiaoa, Qi Menga, Chang Bao Hana, Hui Yana, Yongzhe Zhanga, "Stability of all-inorganic perovskite solar cells", Nano-Energy, 67, 104249 (2020).

[6] Rui Wang, Muhammad Mujahid, Yu Duan, Zhao-Kui Wang, Jingjing Xue, and Yang Yang, "A Review of Perovskites Solar Cell Stability", Advanced Functinal Materials, 1808843, 1-25 (2019).

[7] Mohammad K. Hossain, Pengfei Guo, Wayesh Qarony, Yuen H. Tsang, Chaoping Liu, Sai W. Tsang, Johnny C. Ho, and Kin M. Yu, "Controllable optical emission wavelength in all-inorganic halide perovskite alloy microplates grown by two-step chemical vapor deposition", Nano Research, 13, 2939-2949 (2020).

[8] Xiaoping Wan, Ze Yua, Wenming Tianb , Fuzhi Huang, Shengye Jinb , Xichuan Yanga, Yi-Bing Cheng, Anders Hagfeldt, Licheng Suna, "Efficient and stable planar all-inorganic perovskite solar cells based on high-quality *CsPbBr$_3$* films with controllable morphology", Journal of Energy Chemistry, 46, 8-15 (2020).

[9] Xiaojing Gu, Wanchun Xiang, Qingwen Tian, Shengzhong (Frank) Liu, "Rational surface-defect control via designed passivation for high-efficiency inorganic perovskite solar cells", Angewandte Chemie, 133, 43, 2348-23354 (2021).

[10] Jiaping Wang, Peng Zhao, Ying Hu, Zhenhua Lin, Jie Su, Jincheng Zhang, Jingjing Chang, and Yue Hao, "An Exploration of All-Inorganic Perovskite/Gallium Arsenide Tandem Solar Cells", Solar RRL, 2100121, 1-10 (2021).

[11] Jiang Kun Wang, Hong-Yi Hou, Yan-Qing Li, and Jian-Xin Tang, "Recent advances in interface engeering of all-inorganic perovskite solar cells", Nanoscale Accepted Manuscrit, 12, 17149-17164 (2020).

[12] Lingyan Lin, Linqin Jiang, Ping Li, Hao Xiong, Zhenjing Kang, Baodian Fan, Yu Qiu, "Simulated development and optimized performance of *CsPbI$_3$* based all-inorganic perovskite solar cells", Solar Energy, 198, 454-460 (2020).

[13] M. Bilal Faheen, Bilawal Khan, Chao Feng, M. Umar Farooq, Fazal Raziq, Yequan Xiao, and Yanbo Li, "All-inorganic perovskite soalr cells: Energetics, Key challenges and Strategies toxard commercialization", ACS Energy Letters, 5, 290-320 (2020).

[14] Nahuel Martínez, Carlos Pinzón , Guillermo Casas, Fernando Alvira, Marcelo Cappelletti, "Computational study of inverted all-inorganic perovskite solar cells based on *CsPbI$_X$Br$_{3-X}$* absorber layer with band gap of 1.78 eV", Accelerating the world's research, (2020).

[15] Masood Mehrabian, Sina Dalir, Ghodrat Mahmoudi, Barbara Miroslaw, Maria G. Babashkina, Anna V. Dektereva, and Damir A. Safin, "A Highly Stable All-Inorganic *CsPbBr$_3$* Perovskite Solar Cell", European Journal Inorganic Chemistry, 32, 3699-3703 (2019).

[16] Lingyan Liu, Linqin Jiang, Ping Li,a,b Yu Qiu, and Qiong Yana, "Numerical analysis of inverted-structure perovskite solar cell based on all-inorganic charge transport layers", Journal of Photonics for Energy, 2, 9 (2019).

[17] Zhun Yao, Zhuo Xu, Wangen Zhao, Jingru Zhang, Hui Bian, Yuankun Fang, Yan Yang, and Shengzhong (Frank) Liu, "Enhanced Efficiency of Inorganic *CsPbI$_{3-x}$Br$_x$* Perovskite Solar Cell via Self-Regulation of Antisite Defects", Advanced Energy Materials, 2100403, 1-8 (2021).

[18] Jing Ma, Jie Su,a Zhenhua Lin, Long Zhou,a Jian He, Jincheng Zhang, Shengzhong Liu, Jingjing Chang, Yue Hao, "Improve the oxide/perovskite heterojunction contact for low temperature high efficiency and stable all-inorganic *CsPbI$_2$Br* perovskite solar cells", Nano Energy, 67, 104241 (2020).

[19] Bing Cheng Yu, Chuantian Zuo, Jiangjian Shi, Qingbo Meng, and Liming Ding, "Defect engineering on all-inorganic perovskite solar cells for high efficiency", Journal of Semiconductors, 5, 42 (2021).

[20] Jin Hyuck Heo, Fei Zhang, Chuanxiao Xiao, Su Jeong Heo, Jin Kyoung Park, Joseph J. Berry, Kai Zhu, and Sang Hyuk Im, 'Efficient and Stable Graded $CsPbI_{3-x}Br_x$ Perovskite Solar Cells and Submodules by Orthogonal Processable Spray Coating", Joule, 5, 481-494 (2021).

[21] M.A.A. Nomana, M.S. Islama, M.J. Abdena, M. Arifuzzamana, and M.A. Islamb, "Effect of Acceptor Concentration on Performance of CdTe Solar Cell from Numerical Analysis", International Conference on Innovations in Science, Engineering and Technology (ICISET), (2016).

[22] Saif Ahmed, Farihatun Jannat, Md. Abdul Kaium Khan and Mohammad Abdul Alim, "Numerical development of eco-friendly Cs2TiBr6 based perovskite solar cell with all-inorganic charge transport materials via SCAPS-1D", Optik, 225, 165765 (2021).

[23] Md. Samiul Islam Sadek, Mst. Sarmin Aktar, Md. Foysal Kabir Shimul and Md Ashraful Islam, "Performance analysis of perovsite solar cell with all inorganique hole transport and electron transport layers", The Seu Journal of Electrical and Electronic Engineering (SEUJEEE), 01, 2710-2130 (2021).

Appendix

Table A1. Electronic and photovoltaic properties of PSCs based on graded $CsPbI_{3-x}Br_x$ with different spraying time

Device		Scan Direction	V_{oc} (V)	J_{sc} (mA/cm^2)	FF (%)	PCE (%)
5 s	Best	Forward	1.20	15.55	78.39	14.63
		Reverse	1.20	15.62	79.06	14.82
	30 samples		1.17±0.02	14.96±0.77	74.75±3.28	13.15±1.15
10 s	Best	Forward	1.17	17.32	78.88	15.98
		Reverse	1.17	17.39	79.95	16.27
	30 samples		1.14±0.02	16.51±0.71	75.84±2.71	14.33±1.13
15 s	Best	Forward	1.15	18.03	79.32	16.45
		Reverse	1.15	18.08	80.85	16.81
	30 samples		1.11±0.03	17.24±0.56	76.58±2.67	14.63±1.07
20 s	Best	Forward	1.10	18.42	76.10	15.42
		Reverse	1.10	18.57	77.87	15.91
	30 samples		1.05±0.03	17.62±0.58	73.63±2.73	13.71±1.12